Physics in Medicine & Biology

IPEM Institute of Physics and Engineering in Medicine

PAPER • OPEN ACCESS

Development and characterisation of a radiobiology proton beamline using radiochromic film dosimetry

To cite this article: Carina Marques Coelho *et al* 2026 *Phys. Med. Biol.* **71** 085003

Physics in Medicine & Biology

IPEM Institute of Physics and Engineering in Medicine

OPEN ACCESS

RECEIVED
17 September 2025

REVISED
20 February 2026

ACCEPTED FOR PUBLICATION
18 March 2026

PUBLISHED
15 April 2026

PAPER

Development and characterisation of a radiobiology proton beamline using radiochromic film dosimetry

Carina Marques Coelho[1,2,3,4,*], Pablo de la Fuente Fernández[4], Paula Bononad[4], Sílvia Viñals[4], Célia Tavares de Sousa[4,5], Daniel Galaviz[1,3], Federico Herrera[2,6], Gastón García López[4,7], Inés del Monte-García[8], José Olivares[4,9], Maria Dolores Ynsa Alcala[4,5], Miguel Manso Silván[4,5,7], Daniel Sánchez-Parcerisa[8] and Belén Cortés-Llanos[4,*]

[1] Laboratory of Instrumentation and Experimental Particle Physics, 1649-003 Lisbon, Portugal
[2] BioISI - Biosystems and Integrative Sciences Institute, Faculty of Sciences, University of Lisbon, Lisbon 1749-016, Portugal
[3] Department of Physics, Faculty of Sciences, University of Lisbon, 1749-016 Lisbon, Portugal
[4] Centre for Micro Analysis of Materials, Universidad Autónoma de Madrid, 28049 Madrid, Spain
[5] Department of Applied Physics, Faculty of Sciences, Universidad Autónoma de Madrid, 28049 Madrid, Spain
[6] Department of Chemistry and Biochemistry, Faculty of Sciences, University of Lisbon, 1749-016 Lisbon, Portugal
[7] Fotiónica: Aplicaciones óptico-fotónicas con iones de alta energía, Universidad Autónoma de Madrid, Unidad asociada al Consejo Superior de Investigaciones Científicas por el Instituto de Óptica 'Daza de Valdés', 28049 Madrid, Spain
[8] Grupo de Física Nuclear, EMFTEL, IPARCOS, Universidad Complutense de Madrid, 28040 Madrid, Spain
[9] Instituto de Óptica 'Daza de Valdés', Consejo Superior de Investigaciones Científicas, 28006 Madrid, Spain
[*] Authors to whom any correspondence should be addressed.

E-mail: cicoelho@fc.ul.pt and belen.cortes@uam.es

Keywords: proton therapy, radiobiology, beamline, radiochromic film dosimetry, automation

Abstract

Objective. To develop and optimise a dedicated low-energy proton beamline at the Centre for Micro-Analysis of Materials (CMAM, Madrid, Spain) for radiobiological applications. *Approach.* An automated irradiation system was implemented, integrating Gafchromic EBT3 radiochromic film dosimetry corrected for linear energy transfer dependent quenching and post-irradiation darkening. Dosimetric calibration was performed using multichannel analysis, and beam performance was systematically evaluated as a function of distance, raster scanning area, beam intensity and reproducibility. *Main results.* Optimal operating conditions were identified at moderate beam currents ($\leqslant$1 nA) and scanning areas of 40×40 to 50×50 mm^2, yielding homogeneous dose distributions with reproducibility better than 8%. The dosimetric protocol demonstrated linearity across clinically relevant dose ranges and allowed a reliable correlation between irradiation parameters and absorbed dose. Proof-of-concept experiments on U-87 MG glioblastoma cells confirmed the system's ability to deliver controlled and biologically effective proton exposures, as demonstrated by clonogenic survival assays. *Significance.* These results establish the CMAM implantation beamline as a robust and versatile platform for preclinical proton radiobiology, providing accurate dosimetric control and supporting investigations of relative biological efficacy. The system facilitates translational advances in proton radiobiology, bridging physical and biological studies in low-energy proton irradiation.

1. Introduction

Proton therapy (PT), the most widely used form of charged-hadron therapy, offers superior spatial dose conformity and reduced exposure to surrounding healthy tissues compared to photon or electron therapy (Baratto-Roldán *et al* 2018). Compact commercial systems have accelerated clinical adoption, but evidence of improved patient outcomes is still emerging. Current research aims to model relative biological effectiveness (RBE) as a function of dose, fractionation, tissue type, and linear energy transfer (LET). While clinical PT often assumes a generic RBE of 1.1, the biological effectiveness can vary near the Bragg peak, and LET-guided approaches have been proposed to account for this heterogeneity (Carabe *et al* 2013, Unkelbach *et al* 2017, Constanzo *et al* 2019), underscoring the need for further

radiobiological studies. Low-energy proton beams (typically < 40 MeV) are particularly suitable because they provide high LET values with narrow energy distributions, making them ideal for studying the biological effects of radiation (Baratto-Roldán *et al* 2018, 2020). Such research is crucial to understand the biological responses to proton irradiation and refining both the therapeutic and experimental techniques. Several facilities have developed experimental beamlines optimised for precise irradiation of monolayer cell cultures and other biological targets (Dahle *et al* 2017, Constanzo *et al* 2019, Baratto-Roldán *et al* 2020, Henthorn *et al* 2020, Chaudhary *et al* 2021, Rovituso *et al* 2025).

Dedicated accelerator infrastructures, such as the Centre for Micro-Analysis of Materials (CMAM) tandem system, provide monoenergetic beams in the mid-LET range (1–10 MeV) without the use of energy degraders, thereby ensuring narrow energy spreads and highly reproducible irradiation conditions. This level of control enables systematic investigations of LET-dependent biological responses and supports emerging topics such as RBE variability and ultrahigh-dose-rate effects. These complementary capabilities highlight the continued importance of specialised research beamlines for advancing the fundamental radiobiological knowledge required to refine and translate PT.

Accurate dosimetry is essential to ensure the reliability of dose measurements in radiobiological experiments and clinical applications. Radiochromic film (RCF) dosimetry is a widely used passive technique owing to its submillimetre spatial resolution and robustness (Mijnheer 2017, Niroomand-Rad *et al* 2020, Sanchez-Parcerisa *et al* 2021). The RCFs include different families such as XR-QA, HD-V2, and the EBT series, with Gafchromic EBT3 being commonly employed in PT because of their near-tissue equivalence and reliable performance in proton beam dosimetry (Devic 2011, Niroomand-Rad *et al* 2020, Méndez *et al* 2021). A known limitation is their LET dependence, as films under-respond in high-LET regions owing to quenching, with relative efficiency (RE) decreasing as LET increases (Vadrucci *et al* 2015, Mijnheer 2017, Grilj and Brenner 2018, Vallières *et al* 2019, Resch *et al* 2020, Méndez *et al* 2021). Upon irradiation, RCFs undergo a near-instantaneous colour change, forming permanent images proportional to the absorbed dose, with residual darkening occurring over 24-48 h post-irradiation (Devic 2011, Niroomand-Rad *et al* 2020). The optical density of these films, measured using specific protocols, provided an absolute dose value. The RCF dosimetry systems follow a two-step protocol: calibration and measurement. Calibration involves irradiating films with known doses and generating dose-response curves for each colour channel (Red, Green, Blue - RGB). These curves were later used to determine unknown doses, ensuring consistency in imaging and scanning protocols (Devic 2011, Santos *et al* 2021). Multichannel methods that integrate data from all three RGB channels improve dosimetric accuracy compared with single-channel approaches. The red channel exhibited higher sensitivity at low doses (up to 8-10 Gy), the green channel was more sensitive at higher doses, and the blue channel showed a lower dose gradient across all levels (Lewis *et al* 2012, Santos *et al* 2021). Combining precise dosimetry techniques, such as RCFs, with the unique properties of low-energy proton beams enables highly accurate radiobiological experiments. These efforts are essential to further improve our understanding of radiation biology and to optimise proton irradiation for clinical use.

The objectives of this study were to (*i*) develop and characterise a low-energy proton beamline optimised for radiobiological research, (*ii*) implement and validate an RCF dosimetry protocol with LET-dependent quenching and reading time corrections, (*iii*) assess the dosimetric accuracy and reproducibility of the system for preclinical applications, and (*iv*) demonstrate the feasibility of controlled proton radiobiological experiments through a proof-of-concept clonogenic survival study.

As a first application of this experimental framework, a proof-of-concept radiobiological study was carried out to characterise the clonogenic survival response of U-87 MG glioblastoma cells following proton irradiation. Glioblastoma is the most common and aggressive primary brain malignancy and is characterised by rapid progression and poor prognosis. Conventional therapies, including surgery, radiation therapy, and chemotherapy, remain largely ineffective. Emerging therapeutic approaches, such as PT, have therefore attracted growing interest for their ability to deliver highly conformal radiation doses, enabling precise tumour targeting while minimising damage to surrounding healthy brain tissue (Chambrelant *et al* 2021).

2. Materials and methods

The CMAM facility operates a 5 MV terminal voltage tandem accelerator, designed and built by High Voltage Engineering Europe B. V. (HVEE), in which protons are first accelerated toward the terminal, undergo charge exchange, and are subsequently accelerated a second time away from the terminal, resulting in a final beam energy of 10 MeV. It is equipped with three duoplasmatron sources, primarily used to produce positive (He^+) and negative (H^-) ions. This accelerator is mainly devoted to the analysis

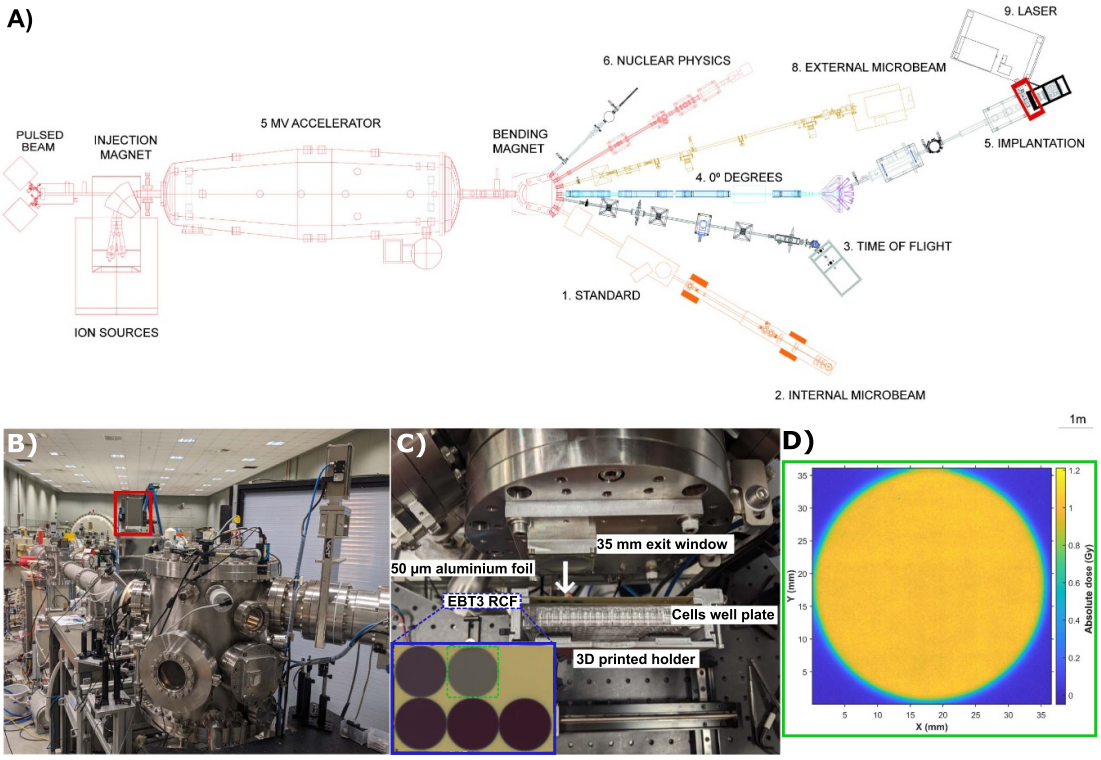

Figure 1. Overview of the experimental setup and irradiation geometry used for proton beam delivery and dosimetry at the CMAM accelerator. (a) Schematic view of CMAM accelerator showing the six beamlines, with the IMP beamline indicated as number 5. The position of the Faraday Cup (FC) used for beam current monitoring is indicated by the red rectangle. (b) Detailed view of the IMP beamline, with the FC again indicated by the red rectangle. (c) Top view of the setup for proton irradiation, including the 50 μm-thick aluminium foil, the EBT3 radiochromic film (RCF), and the cell culture well plate mounted on the 3D-printed holder. The white arrow indicates the direction of the proton beam through the system. The blue inset shows an example of an RCF obtained during the calibration procedure prior to the biological experiments, and the green rectangle marks the region corresponding to the analysed irradiation field. (d) Two-dimensional absolute dose map obtained from the analysis of the region indicated by the green rectangle in panel (c), corresponding to the lowest irradiation time used in the calibration (2 s), illustrating the spatial dose distribution across the analysed irradiated field.

and modification of materials and operates six beamlines (Redondo-Cubero *et al* 2021). For the present study, the implantation (IMP) beamline was adapted for the radiobiological proton irradiation experiments as described below.

2.1. Beamline for proton radiobiology

The CMAM IMP beamline is positioned at -20 ° relative to the tandem accelerator axis, after the second switching magnet, and has a total length of 6 m (figure 1(a)). The irradiation chamber was electrically isolated and designed for ultra-high vacuum conditions (figure 1(b)). The beam fluence was monitored by measuring the current values using a Faraday Cup (FC) positioned upstream of the window for beam extraction to air (figures 1(a) and (b) highlighted by the red rectangle). Under vacuum conditions, irradiation can be performed with a homogeneous beam covering large areas of up to $100 \times 100\,\mathrm{mm}^2$, facilitated by a fast electrostatic beam raster system provided by HVEE. The proton beam exits the vacuum chamber through an exit window with a diameter of 35 mm and covered by an aluminium foil of 50 μm thickness (figure 1(c), white arrow). Under all irradiation conditions used in this study, the accelerator delivers a continuous (non-pulsed) proton beam.

A fully automated three-dimensional (3D) motorised stage was developed for high-precision multiposition irradiation of cell cultures, providing 10 μm positioning accuracy (figure 1(c)). The motion is controlled by NEMA11 stepper motors coupled with TMC2209 drivers (1/64 microstepping) and an MKS TinyBee controller board running Marlin firmware, operated via G-code instructions.

Homogeneous irradiation was achieved with the IMP beamline raster system, which scans the beam along both axes at suitable frequencies (x axis: 31 Hz and y axis: 2 kHz) to prevent aliasing, thereby ensuring uniform coverage of the sample area within milliseconds. In the IMP chamber, the beam exit window is positioned downstream of the scanning system, as previously described. After configuring the raster system to encompass this window, the samples were positioned on the motorised stage (figure 1(c)) and irradiation time is manually controlled using an FC located in the low-energy section

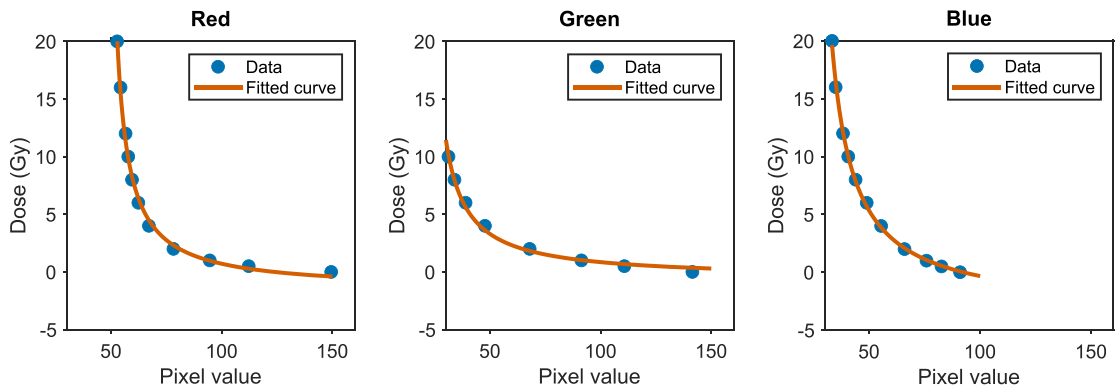

Figure 2. Dose–response calibration curves for the red, green, and blue channels.

Table 1. Calibration parameters for each colour channel

Parameters	Red	Green	Blue
a	-1.396×10^{0}	-4.751×10^{-1}	-3.529×10^{0}
b	1.175×10^{2}	1.039×10^{2}	2.416×10^{2}
c	4.388×10^{1}	1.964×10^{1}	2.184×10^{1}

of the accelerator. The resulting spatial dose distribution across the analysed irradiation field is illustrated by the two-dimensional absolute dose map shown in figure 1(d). An uncertainty of $\pm$ 0.25 s, determined from repeated measurements of the operator's manual switching response time, was incorporated into all dose calculations. A new system using a fast electrostatic deflector and a custom interface is under development for automated time control.

2.2. Dosimetry with RCFs

All dose measurements in this study were performed using Gafchromic^{TM} EBT3 films (Ashland Inc.). For calibration, RCFs were irradiated at the Hospital General Universitario Gregorio Marañón (Madrid, Spain) using a uniform 6 MV photon beam from an Elekta Versa HD linear accelerator, with a uniform $10 \times 10\,cm^2$ field at 10 cm depth. The delivered doses were 0, 0.5, 1, 2, 4, 6, 8, 10, 16, and 20 Gy, measured and referenced against an FC-65G ionization chamber (Serial 4148). RCFs were scanned using an Epson CX4500 flatbed scanner at 300 dpi resolution. Each film was placed at the geometric centre of the scanner, which corresponds to the region of highest spatial uniformity as reported by Saur and Frengen (2008), with the irradiated side facing the glass. The scanner was pre-warmed with three blank scans and cleaned between runs, and images were saved in tagged image file format. To ensure consistent optical development, all calibration and characterisation RCFs were scanned 24 h after irradiation. For the quick scan factor (QSF) analysis, films were additionally scanned within the first 60 min to quantify post-irradiation darkening. For biological irradiations, a single early scan at approximately 5 min post-exposure was used with the QSF function to determine the irradiation time required to reach the target dose. These films were rescanned after 24 h, and the final dose values were corrected accordingly. The RCFs used for the characterisation were scanned multiple times using alternative mounting approaches to ensure full contact with the glass surface and to eliminate artefacts from air gaps. No systematic differences were observed between repeated scans. Measurements were only taken from the central region of the film to minimize the effect of scanner lateral non-uniformity. A MATLAB script was developed to analyse the calibration RCFs, computing the mean and standard error of the mean (SEM) of the relative pixel values (PV) as a function of the dose (D) across the RGB colour channels. The calibration of the RCFs is described by the function:

$$D = a + \frac{b}{\mathrm{PV} - c} \tag{1}$$

where a, b, and c are the fitting coefficients, representing baseline offset, curve scaling factor, and pixel value shift, respectively (Sanchez-Parcerisa *et al* 2021). After the calibration RCFs were processed, the script generated the corresponding calibration curves (figure 2) and fitting parameters (table 1).

The experimental RCFs were scanned following the same protocol as the calibration films (Devic 2011, Santos *et al* 2021) and analysed using a separate MATLAB script. A fixed circular region of interest

(ROI) with a diameter of 10 mm was then drawn at the geometric centre of the irradiated field and applied consistently to all RCFs. This approach ensures that a uniform physical area is analysed in each RCF, minimising artefacts from scanner non-uniformity and excluding field edges affected by the lateral penumbra. The central region of the beam was selected because it provides the highest uniformity in intensity and energy after passing through the exit window and air gap. This method reduces uncertainties associated with dose fall-off and scattering and follows established proton dosimetry practices that use small, central ROIs to obtain reproducible and representative dose measurements (Kirby *et al* 2011, Karsch *et al* 2012, Howard *et al* 2020). A sensitivity analysis was also performed to assess the dependence of the coefficient of variation on different ROI diameters, confirming that a 10 mm ROI provided an optimal balance between measurement precision and spatial specificity.

The script calculates the average dose and SEM for each colour channel individually and for the combined RGB channels. For each channel, the dose was derived from the mean pixel intensity within the selected ROI using the calibration constants listed in table 1. Measurement uncertainties were propagated from the pixel-value variance, and the SEM was used as the reported uncertainty in all results, calculated as $\mathrm{SEM} = \mathrm{SD}/\sqrt{N}$, where N is the number of pixels within the ROI. The overall calibrated dose was obtained as a multichannel estimate, quantified through inverse-variance weighting of the individual RGB channel doses. This approach provides a statistically meaningful estimate of the uncertainty of the mean dose, improving precision while reducing channel-specific noise and artefacts across all dose–response analyses.

Since the RCF response to proton irradiation is LET-dependent, a correction model was implemented following the approach described by Sanchez-Parcerisa *et al* (2021). The RE associated with LET quenching was derived using the fitting parameters reported for Gafchromic^{TM} EBT3 films. The LET at the film surface was computed as a function of the residual proton energy after transmission through the exit window and air gap, using the same model and coefficients described in that work. The only modification introduced in this study concerned the energy-loss description through the 50 μm aluminium extraction foil, for which the parameters $s = 2.2717\,\mathrm{MeV}^{1.73}$ and $q = -0.699$ were applied. These parameters account for the specific energy degradation conditions of the CMAM IMP beamline, ensuring accurate LET estimation prior to dose correction.

To assess the suitability of the IMP beamline for biological sample irradiation, the average dose measurements were performed under various beam conditions. These data facilitated the development of an online dosimetry system capable of calibrating the delivered dose as a function of the beam intensity, exposure time, distance from the exit window, and raster-defined scanning area. Reproducibility tests confirmed that identical doses can be reliably delivered across multiple samples and experiments. For data validation, the records of the measured ion beam current over time (charge files) were examined to verify the irradiation duration. When discrepancies between the planned and actual irradiation times were detected, corrections were applied to ensure an accurate analysis. An uncertainty of $\pm$ 0.25 s, determined from the experimenter's reaction time, was incorporated into the calculations.

2.3. Proof-of-concept study: proton irradiation of tumor cells

After the dosimetric characterisation of the IMP beam line at the CMAM, a series of experiments were conducted. The characteristics of the irradiated cell lines, along with the protocols followed for cell culture, seeding, irradiation, and clonogenic assays are detailed in the following sections.

2.3.1. Cell culture and proton irradiation conditions

U-87 MG glioma cells (ATCC® HTB-14) were maintained in High Glucose Dulbecco's Modified Eagle Medium (DMEM) (Cytiva, Marlborough, MA, USA) supplemented with 10% fetal bovine serum (Cytiva) and 1% penicillin–streptomycin (P/S) (Thermo Fisher Scientific, Waltham, MA, USA) under standard culture conditions (37 °C, 5% CO_2). At confluence, the cells were rinsed with 1× phosphate-buffered saline (PBS), detached using 0.05% trypsin (Thermo Fisher Scientific), resuspended in fresh complete medium, and counted. A total of 5000 cells were seeded in ibiTreat 96-well plates and incubated for 24 h before irradiation under standard conditions.

Irradiation was performed with a 10 MeV proton beam extracted through the exit window into air, with the beam current at the FC near the window set to 0.5–1 nA. A calibration RCF was first irradiated to determine the dose rate, corrected for timing (section 3.2), and subsequently used to calculate the exposure times for the planned doses. The cell plates were then placed 4 cm downstream, perpendicular to the beam axis, with an additional RCF positioned in front to verify the delivered dose. Each irradiation covered a 35 mm-diameter circular field encompassing the 12 fully irradiated wells, while one area was reserved as a non-irradiated control (figure 1(c)). Twenty-four hours post-irradiation, the RCFs were

scanned and the dosimetric characterisation was performed using a ROI covering the full irradiated field, corresponding to the area exposed during the biological experiments.

2.3.2. Clonogenic assay

A clonogenic assay was performed 48 h after irradiation to ensure that colony formation exclusively reflected irradiation-induced effects (Franken *et al* 2006). For each irradiation condition, three biological samples were prepared per dose group. Each sample was subsequently seeded into three separate wells of a 6-well plate (three technical replicates per sample), resulting in a total of nine wells analysed per dose condition. For each experimental condition, the cells were trypsinized, centrifuged at 1300 rpm for 5 min, resuspended in DMEM, and seeded at a density of 1000 cells per well in 6-well plates. Cultures were incubated for 10 d under standard conditions to allow colony formation. The colonies were then fixed and stained with crystal violet (0.125 mg in 10 ml of ethanol (70%) and 40 ml of distilled water; Thermo Fisher) for 10 min at room temperature, followed by three washes with PBS (1x). The plates were scanned and the colonies were counted. The plating efficiency (PE) was calculated as the ratio of colonies formed to the number of cells seeded:

$$\mathrm{PE}\,(\%) = \frac{n_{\text{colonies formed}}}{n_{\text{cells seeded}}} \times 100 \tag{2}$$

The survival fraction (SF) was then determined as described by Munshi *et al* (2005):

$$\mathrm{SF} = \frac{PE_{\text{irradiated}}}{PE_{\text{control}}}. \tag{3}$$

3. Results

3.1. Optimisation of the irradiation parameters

Following the methods described in section 2.4, we developed protocols to evaluate the dependence of the deposited dose on the distance from the exit window, determine the optimum scanning area for sample irradiation, and assess the reproducibility of the dose as a function of beam intensity and irradiation time.

3.1.1. Dose-time dependence and sample-distance assessment

To evaluate the dependence of the delivered dose on irradiation time, measurements were performed at a fixed distance of 40 mm from the exit window while keeping the beam intensity (0.5 nA) and scanning area ($40 \times 40\,\mathrm{mm}^2$) constant. The resulting average doses, corrected for the timing uncertainty of ± 0.25 s, are shown in figure 3. A linear fit was applied to these data to confirm proportionality between dose and exposure time under these conditions. The results indicate that the time–dose relationship remains linear over the tested interval, supporting the use of exposure time as a reliable parameter for dose control in biological irradiations, although the SEM increases at longer exposures due to partial RCF saturation.

The influence of the sample distance was evaluated separately by irradiating RCFs at 40, 50, 60, and 70 mm from the exit window, using a beam intensity of 0.8 nA and exposure times of 2, 5, 10, and 15 s. For each distance, a linear fit of dose versus time was used to obtain the corresponding average field dose rate and expected fluence rate (table 2). The resulting dose rates vary only slightly across the tested distances, remaining compatible with statistical uncertainties. These small differences are consistent with the modest increase in stopping power and range-straggling effects expected as the air gap increases.

3.1.2. Determination of the optimal scanning area

The irradiation of the RCFs used to analyse dose variation as a function of the scanning area was performed at a distance of 40 mm from the exit window, with a beam intensity of 1.1 nA, an exposure time of 5 s. Ten different scanning areas (obtained by the movement of the beam raster) were tested (figure 4). For the smallest scanning areas, the field shape in the RCF images appears slightly rectangular due to the projection of the rastered beam through the circular exit window and minor geometrical effects near the beam boundaries, rather than any intrinsic asymmetry of the scanned field.

The calculated average dose decreased with increasing scanning area (figure 5(a)). For the $60 \times 60\,\mathrm{mm}^2$ scanning area, the irradiation time was inadvertently longer, as observed by the accelerator charge files, and the measured dose was corrected proportionally to the actual exposure time. For the two smallest scanning areas (10×10 and $15 \times 15\,\mathrm{mm}^2$), the SEM values were notably high. The lowest SEM values were observed for scanning areas above 40×40 (figure 5(b)).

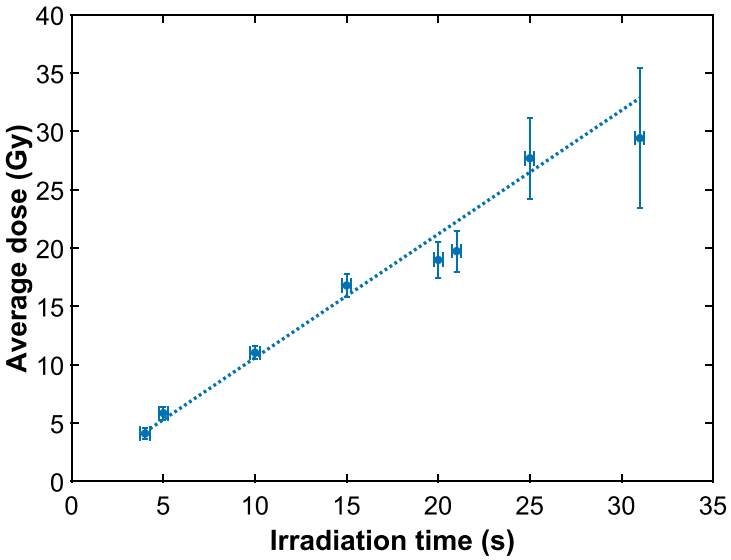

Figure 3. Average dose as a function of the irradiation time, assuming a constant timing uncertainty of ± 0.25 s. The dotted line represents the linear fit to the data.

Table 2. Calculated average field dose rates (total dose in the analysed ROI divided by irradiation time) based on the linear regression, and corresponding expected fluence rates at various distances

Distance (mm)	Dose rate from linear regression (Gy s^{-1})	Expected fluence rate (protons mm^{-2} s^{-1})
40	0.45 ± 0.01	4.7 ± 0.1
50	0.46 ± 0.01	4.7 ± 0.1
60	0.43 ± 0.01	4.4 ± 0.1
70	0.44 ± 0.01	4.6 ± 0.1

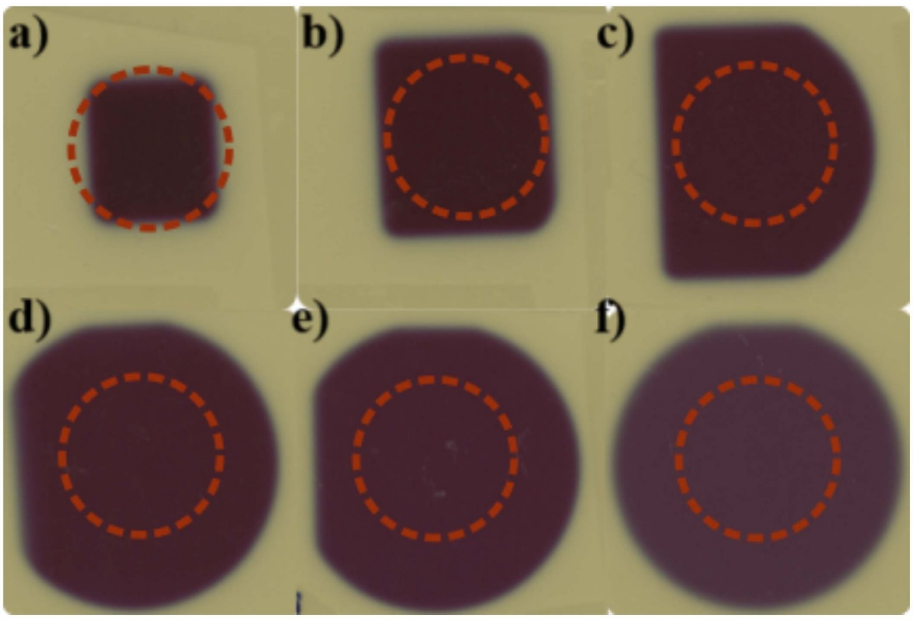

Figure 4. RCF images for scanning areas: (a) 10 × 10 mm^2, (b) 15 × 15 mm^2, (c) 20 × 20 mm^2, (d) 25 × 25 mm^2, (e) 30 × 30 mm^2 and (f) 40 × 40 mm^2. ROIs used for dose averaging are shown. Areas $\geqslant$ 40 × 40 mm^2 show similar profiles due to the exit window limit.

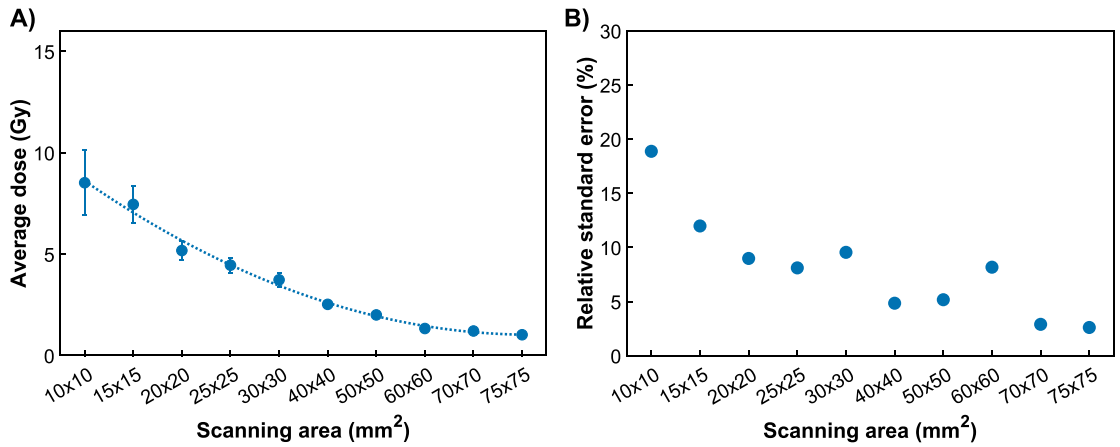

Figure 5. (a) Calculated average dose as a function of the scanning area for a fixed irradiation time of 5 s and a beam current of 1.1 nA, The data are fitted to a 2nd degree polynomial function. (b) Relative error deviation as a function of the scanning area under the same irradiation conditions, used as an indicator of field uniformity.

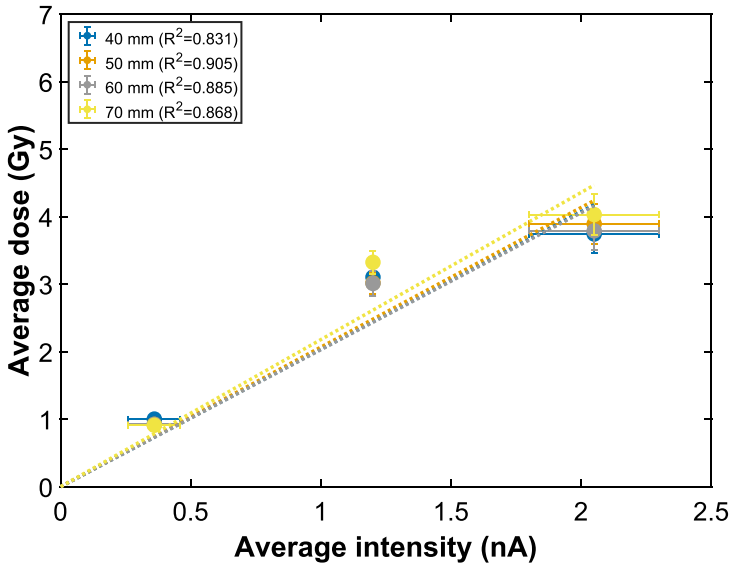

Figure 6. Calculated average dose as a function of the average beam intensity measured by the external FC, for various distances from the exit window, fitted to a linear function and with the corresponding R^2 values shown in the legend.

Consistent with previous studies (Lewis *et al* 2012), the red channel of EBT3 films provides the highest sensitivity and lowest uncertainty at low doses, making it preferable for small-field analysis. However, to maintain consistency across all datasets, a multichannel analysis approach was used throughout this work. In addition, scanning areas larger than $40 \times 40\,mm^2$, ideally covering the full exit window, are recommended to achieve improved field homogeneity.

3.1.3. Intensity

To analyse the influence of the beam intensity on the delivered dose, the exposure time (5 s) and scanning area ($40 \times 40\,mm^2$) were kept constant. The irradiation was performed at four distances (40, 50, 60, and 70 mm), each tested with three beam intensities (0.45, 1.2, and 2.3 nA). The graphically represented intensities (figure 6) correspond to the average values measured immediately before and after irradiation. The absorbed dose increased with the beam current, but a higher variability was observed in the RCFs exposed to higher intensities.

3.1.4. Reproducibility

To analyse the reproducibility of the dosimetric system, the distance (40 mm) and beam intensity (1 nA) were kept constant. Two different exposure times (5 and 10 s) and two scanning areas (20×20 and

Table 3. Calculated dose rates for each repetition (shot) and the corresponding scanning area, irradiation time and average dose

Shot	Scanning area (mm^2)	Irradiation time (s)	Average dose (Gy)	Dose rate ($Gy\,s^{-1}$)
1^{st}	40×40	5.00 ($\pm$0.25)	2.3 ($\pm$0.1)	0.46 ($\pm$0.03)
	20×20	10.00 ($\pm$0.25)	16.7 ($\pm$2.3)	1.67 ($\pm$0.24)
2^{nd}	40×40	5.00 ($\pm$0.25)	2.4 ($\pm$0.1)	0.48($\pm$0.03)
	20×20	10.00 ($\pm$0.25)	15.4 ($\pm$2.0)	1.54 ($\pm$0.21)
3^{rd}	40×40	5.00 ($\pm$0.25)	2.5 ($\pm$0.1)	0.50 ($\pm$0.02)
	20×20	10.00 ($\pm$0.25)	17.7 ($\pm$2.6)	1.77 ($\pm$0.26)

$40 \times 40\,mm^2$) were tested and irradiation was repeated three times for each condition. The corresponding dose rates were calculated for each RCF and are presented in table 3.

Under identical scanning areas and irradiation times, the dose rate remained nearly constant across repetitions, with a coefficient of variation of 6%-8%, confirming that the beamline and dosimetric system can reliably reproduce radiation doses. This level of reproducibility is essential for the accurate execution of biological irradiation experiments.

3.2. Dosimetry

RCFs are known to continue darkening for several hours after irradiation (Devic *et al* 2005), and standard protocols recommend a 24-48 h waiting period to ensure accurate dose measurements. However, in our protocol (section 2.2), the dose rate was determined as part of the daily beam quality assurance at the start of each experimental shift, requiring RCFs to be scanned shortly after irradiation. To account for post-irradiation darkening, a correction factor was established by scanning the selected films immediately after irradiation and again after at least 24 h. The ratio between the measured dose rates from these two time points was defined as the *QSF*, and was calculated as follows:

$$\mathrm{QSF}(t) = \frac{\dot{D}(t_2)}{\dot{D}(t_1)} \tag{4}$$

where $\dot{D}(t_2)$ is the dose rate measured at least 24 h after irradiation and $\dot{D}(t_1)$ is the dose rate measured at time t post-irradiation.

Ten different QSF measurements were performed within the first 60 min after irradiation using dose values in the 0-12 Gy range. Six dose spots were evaluated for each measurement to determine the dose rate. The resulting data were empirically fitted and the QSF as a function of the elapsed time t (in minutes) is expressed as

$$\mathrm{QSF}(t) = 1.211 - 0.0415 * ln(t)\,. \tag{5}$$

This equation is valid for immediate scanning (times shorter than 60 min). For scans performed between 1 h and 8 h after irradiation, a constant value of QSF = 1.04 was employed. This value is based on previous experiments performed with photon beams and was found to be consistent with the trend observed in the present data. Because most films in this work were scanned shortly after irradiation, measurements beyond 1 h were not further investigated. An overall 2% uncertainty in the QSF is considered a conservative estimate and has been included in the global uncertainty budget. The fitted curves and measurement data are shown in figure 7.

3.3. Automated proton irradiations on glioblastoma cells

Automated proton irradiation was performed using a motorized stage specifically designed to position both the RCF and the biological sample at the same irradiation site (figure 1(c)). U-87 MG cells were irradiated with doses of 0 (control), 4.1 ± 0.2, and 12.6 ± 0.4 Gy, delivered at a dose rate of $0.6\,Gy\,s^{-1}$. RCFs were scanned 24 h after irradiation to verify the radiation dose delivered to the cells. We performed a clonogenic assay, which evaluates the ability of individual cells to proliferate and form colonies *in vitro*, to study the long-term viability of cells and provide critical insights into cellular radiosensitivity and treatment efficacy. The number of colonies formed and the SF of the control and those irradiated at 4.1 and 12.6 Gy are shown in figure 8(a).

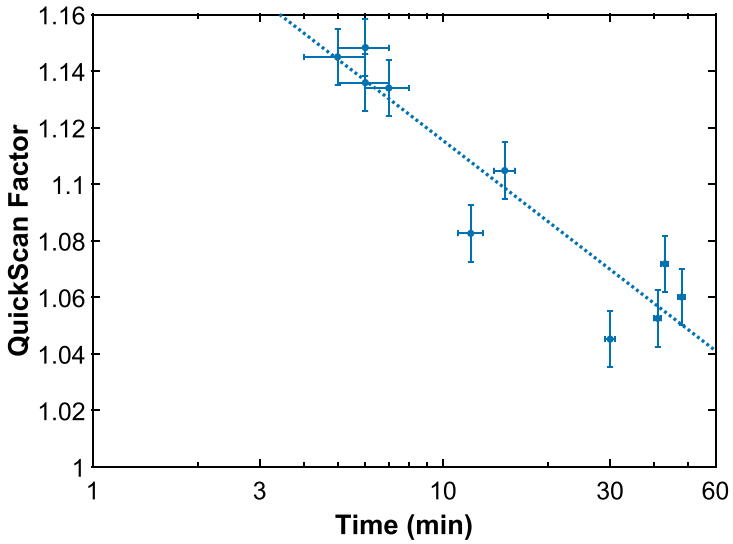

Figure 7. Measured values of the QSF for various times after irradiation. The dotted line shows the result from the considered logarithmic function.

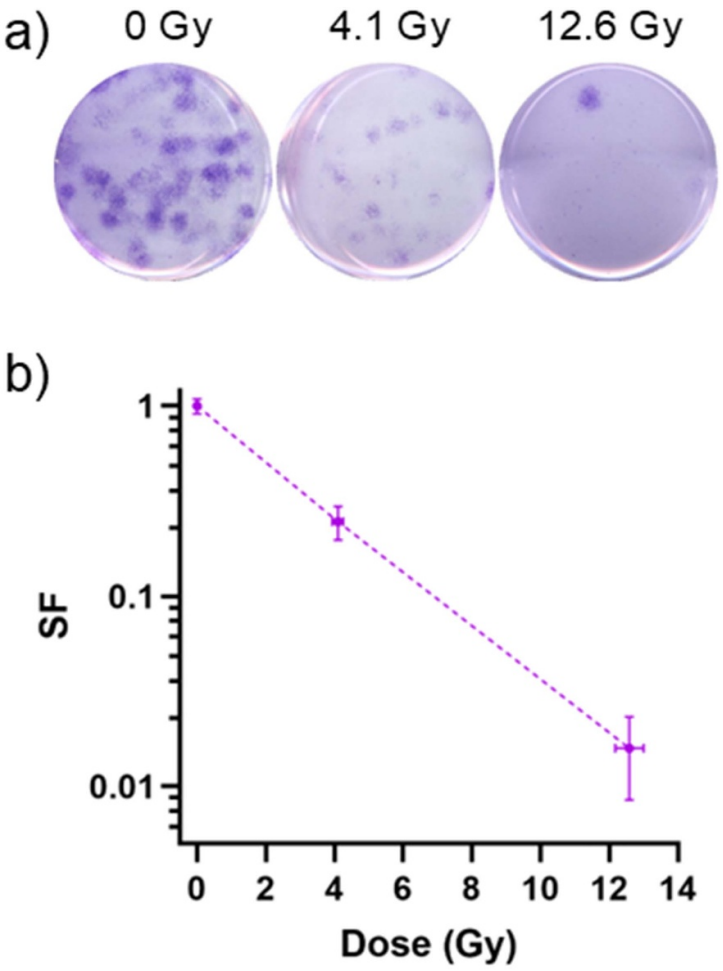

Figure 8. (a) Images of the number of colonies and (b) Survival Fraction (SF) of U-87 MG cells after 0, 4.1 and 12.6 Gy proton irradiations with the trend line represented.

4. Discussion

The developed proton beamline provided reliable dose delivery and homogeneity suitable for radiobiological studies, meeting key requirements identified for modern preclinical irradiation platforms, including recent multi-accelerator infrastructures designed to ensure reproducible and well-characterised biological exposures (Bin *et al* 2022, Metzkes-Ng *et al* 2023, Rovituso *et al* 2025). RCF dosimetry with LET-dependent corrections enabled accurate measurements of low-energy proton fields, consistent with reports emphasizing the need to account for LET effects to avoid dose underestimation (Dahle *et al* 2017, Grilj and Brenner 2018, Resch *et al* 2020). The beam reproducibility and dose linearity achieved are consistent with results reported for other preclinical proton radiobiology platforms, including compact or low-energy setups and clinical research beamlines adapted for biological studies (Romano *et al* 2016, Henthorn *et al* 2020, Bin *et al* 2022, Horst *et al* 2025, Rovituso *et al* 2025). Homogeneous dose delivery across the irradiation field is particularly important for studies involving monolayer cell cultures or small animal models, as highlighted by recent advances in beam shaping, field definition and dosimetric control in preclinical radiobiology platforms (Baratto-Roldán *et al* 2020, Brack *et al* 2020, Suckert *et al* 2021, Metzkes-Ng *et al* 2023).

Small scanning areas produce higher SEM in dose measurements, likely due to beam non-uniformity, edge effects, and local film heterogeneities (Gonzalez-Lopez *et al* 2015, Clausen *et al* 2023). However, enlarging the scanned region does not improve the precision indefinitely. Instead, an optimal scanning area, typically above 40×40, minimizes the SEM by balancing sufficient statistical sampling with reduced exposure to peripheral non-uniformities or LET effects (Battaglia *et al* 2016, Kato 2019). Larger areas may include regions affected by proton scattering and dose fall-off near the field edges, highlighting the need to select an appropriately sized intermediate region for radiobiological dosimetry.

In this study, beam intensities above approximately 1 nA led to increasingly irregular dose delivery, resulting in a loss of linearity between the set current and the measured average dose, with significantly greater variability observed in the 2.0-2.5 nA range. These fluctuations reflect the unstable beam output at higher currents, compromising the accuracy and repeatability of irradiation. Maintaining the beam intensity at or below 1 nA mitigated these effects ensuring stable currents. Instabilities may likely come from the ion source operation. However, the exploration of higher beam currents is foreseen for the future, including consultation with the supplier of the accelerator systems.

The observed 6%-8% variation in repeated dose measurements reflects the combined uncertainty of beam stability, film response, and data analysis. In our configuration, the dominant contribution to this variability arises from irradiation timing and monitoring procedure rather than from the intrinsic stability of the tandem accelerator. Beam on/off control was performed manually, and repeated timing measurements showed an operator-dependent timing uncertainty of $\pm$ 0.25 s, which constitutes a significant fraction of the delivered dose for short irradiations. In addition, the FC upstream of the exit window provides an integrated current value but does not record real-time fluctuations during the exposure, which limits its precision for dose prediction. Automated time control and the implementation of an online transmission-mode beam monitor are currently being introduced to reduce these uncertainties. While the present reproducibility is adequate for beamline characterization and proof-of-concept biological experiments, uncertainties below 5% are desirable for accurate RBE assessment (Friedrich *et al* 2012, McNamara *et al* 2015). Further optimization of beam monitoring at CMAM is therefore expected to improve measurement consistency in future studies. For proton irradiation, we usually work between 0.5-1 nA, where there is a linear behaviour. The intensity fluctuations were corrected by measuring the intensity at the beginning and end of each irradiation set.

The integration of computational modelling (e.g. Monte Carlo simulations) further strengthens the reliability of the system by enabling the detailed characterisation of LET distributions and dose deposition, which are critical for interpreting biological outcomes and for future investigations into variable RBE models (Dahle*et al* 2017, Jones *et al* 2018). Proof-of-concept experiments with U-87 MG glioblastoma cells confirmed that the proton doses delivered by the adapted beamline produced a measurable and biologically meaningful reduction in clonogenic survival. The SF values obtained in this study, 0.25 at 4.1 Gy and 0.016 at 12.6 Gy, show a clear dose-dependent loss of reproductive capacity. These values are consistent with previously published proton irradiation data for U-87 MG cells. In particular, (Cammarata *et al* 2019) reported an SF of $\sim$0.26 at 4 Gy, and the proton survival curve presented by Xiao *et al* (2019), shows SF values of $\approx$ 0.01-0.02 at 10 Gy. The very low survival observed at 12.6 Gy is therefore in line with the expected biological response at high dose and may also reflect the increased uncertainty of RCFs in the high-dose region. The agreement between our measurements and the literature supports the accuracy of the delivered dose and demonstrates that the beamline is suitable for controlled radiobiological studies. Overall, this work contributes to the growing body of evidence supporting

the need for precise, versatile proton irradiation systems in radiobiological research, facilitating more accurate studies on the biological effectiveness of proton irradiation, supporting future clinical translation (Jones *et al* 2018).

5. Conclusions

An automated stage and software were developed to enable precise and reproducible cellular irradiation at the IMP beamline of the CMAM. Analysis of the irradiation results confirmed that the beam intensity, exposure time, and scanning area are the primary determinants of dose delivery. The distance from the exit window showed minimal impact on the measured dose, reflecting a balance between the slight increase in LET with air path length and the concurrent reduction in fluence caused by beam divergence and scattering. Beam intensity fluctuations present notable experimental challenges, directly influencing measurement reproducibility as evidenced by repeatability test data.

The RCF dosimetry system provides reliable and user-friendly dose-rate determination. However, residual variability may stem from operator inexperience in RCF handling, a known critical factor for measurement consistency according to the established literature. ROI selection introduces inherent user-dependent variability, although this was mitigated through standardised selection protocols as detailed in the methodology. Future work will focus on developing new software to analyse scanned RCFs, enabling the real-time monitoring and control of irradiation homogeneity. Moreover, we are improving the stage control software to enable full synchronization between the irradiation times and stage movement, allowing complete automation of the irradiation process.

The CMAM IMP beamline proved to be suitable for homogeneous cell irradiation, consistently producing uniform radiation spots. The system enables the precise control of critical parameters, facilitating accurate dose delivery optimisation, as confirmed by clonogenic assay results with U-87 MG cell irradiation.

Acknowledgments

This research was partially funded by FCT—Fundação para a Ciência e a Tecnologia, I P, Portugal, ProtoTera Grant—PRT/BD/151545/2021, Centre Grant to LIP LA/P/0016/2020, UID/04046/2025 - Biosystems and Integrative Sciences Institute Centre Grant (https://doi.org/10.54499/2023.14971.PEX), FCT/Mobility/1309428002/2024-25 and RE-C06-i06-m02 - 'Reforço do financiamento de Parcerias Internacionais em Ciência, Tecnologia e Inovação'. This Project has received funding from the European Union under the Euratom program, Horizon 2020 under Grant agreement n° 101060008 (OFFERR Platform). The authors appreciate the support of the ENEN2plus mobility Grant, funded by the European Union under the Euratom Research and Training Program. The views and opinions expressed are those of the authors only and do not necessarily reflect those of the European Union or the European Commission. Neither the European Union nor the granting authority can be held responsible for them. It was also partially funded by Comunidad de Madrid under Projects S2022/BMD-7434 ASAP-CM and PR27/21-014, and by the Agencia Estatal de Investigación under Projects PLEC2022-009256, PID2022-141080OB-C22, PID2022-142417OB-I00 (funded by MCIN/AEI/10.13039/501100011033), and CNS2024-154729. The authors acknowledge the support from CMAM-UAM for the beam time (IMP007/23 and IMP020/24) and the technical staff. C T d S acknowledges the program Atraccion de Talento (Comunidad Autonoma de Madrid), reference 2020-T1/IND-19889. Some of the results presented in this work were derived from the research conducted under the F11024 Coordination Research Project.

Data availability statement

The custom scripts developed for data analysis and dosimetry validation are considered integral components of the internal manuals and standard operating procedures at CMAM and, therefore, are available upon reasonable request to the authors rather than through open public repositories. The data that support the findings of this study are available upon reasonable request from the authors.

Conflicts of interest

The authors declare that they have no known competing financial interests or personal relationships that could have influenced the work reported in this study.

ORCID iDs

Carina Marques Coelho 0000-0003-3305-6775
Pablo de la Fuente Fernández 0009-0002-6138-3618
Paula Bononad 0009-0007-8879-734X
Sílvia Viñals 0000-0002-8480-4377
Célia Tavares de Sousa 0000-0003-2879-0051
Daniel Galaviz 0000-0003-2992-4496
Federico Herrera 0000-0002-9596-9353
Gastón García López 0000-0002-1866-4871
Inés del Monte-García 0009-0000-0496-5107
José Olivares 0000-0003-1775-9040
Maria Dolores Ynsa Alcala 0000-0002-7624-0794
Miguel Manso Silván 0000-0002-5063-1607
Daniel Sánchez-Parcerisa 0000-0002-2245-9539
Belén Cortés-Llanos 0000-0002-8069-4908

References

Baratto-Roldán A, del Carmen Jiménez-Ramos M, Battaglia M C, García-López J, Gallardo M I, Cortés-Giraldo M A and Espino J M 2018 Feasibility study of a proton irradiation facility for radiobiological measurements at an 18 MeV cyclotron *Instruments* **2** 26

Baratto-Roldán A, del Carmen Jiménez-Ramos M, Jimeno S, Huertas P, García-López J, Gallardo M I, Cortés-Giraldo M A and Espino J M 2020 Preparation of a radiobiology beam line at the 18 MeV proton cyclotron facility at CNA *Phys. Med.* **74** 19–29

Battaglia M C, Schardt D, Espino J M, Gallardo M I, Cortés-Giraldo M A, Quesada J M, Lallena A M, Miras H and Guirado D 2016 Dosimetric response of radiochromic films to protons of low energies in the Bragg peak region *Phys. Rev. Accel. Beams* **19** 064701

Bin J *et al* 2022 A new platform for ultra-high dose rate radiobiological research using the BELLA PW laser proton beamline *Sci. Rep.* **12** 1484

Brack F-E *et al* 2020 Spectral and spatial shaping of laser-driven proton beams using a pulsed high-field magnet beamline *Sci. Rep.* **10** 9118

Cammarata F P *et al* 2019 Proton therapy and src family kinase inhibitor combined treatments on U87 human glioblastoma multiforme cell line *Int. J. Mol. Sci.* **20** 4745

Carabe A, España S, Grassberger C and Paganetti H 2013 Clinical consequences of relative biological effectiveness variations in proton radiotherapy of the prostate, brain and liver *Phys. Med. Biol.* **58** 2103–17

Chambrelant I, Eber J, Antoni D, Burckel H, Noël G and Auvergne R 2021 Proton therapy and gliomas: a systematic review *Radiation* **1** 218–33

Chaudhary P, Milluzo G, Ahmed H, Odlozilik B, McMurray A, Prise K M and Borghesi M 2021 Radiobiology experiments with ultra-high dose rate laser-driven protons: methodology and state-of-the-art *Front. Phys.* **9** 624963

Clausen M, Ruangchan S, Sotoudegan A, Resch A F, Knäusl B, Palmans H and Georg D 2023 Small field proton irradiation for *in vivo* studies: potential and limitations when adapting clinical infrastructure *Z. Med. Phys.* **33** 542–51

Constanzo J, Vanstalle M, Finck C, Brasse D and Rousseau M 2019 Dosimetry and characterization of a 25-MeV proton beam line for preclinical radiobiology research *Med. Phys.* **46** 2356–62

Dahle T J, Rykkelid A M, Stokkevåg C H, Mairani A, Görgen A, Edin N J, Rørvik E, Fjæra L F, Malinen E and Ytre-Hauge K S 2017 Monte carlo simulations of a low energy proton beamline for radiobiological experiments *Acta Oncol.* **56** 779–86

Devic S 2011 Radiochromic film dosimetry: past, present and future *Phys. Med.* **27** 122–34

Devic S, Seuntjens J, Sham E, Podgorsak E B, Schmidtlein C R, Kirov A S and Soares C G 2005 Precise radiochromic film dosimetry using a flat-bed document scanner *Med. Phys.* **32** 2245–53

Franken N A P, Rodermond H M, Stap J, Haveman J and van Bree C 2006 Clonogenic assay of cells in vitro *Nat. Protocols* **1** 2315–9

Friedrich T, Scholz U, Elsässer T, Durante M and Scholz M 2012 Systematic analysis of rbe and related quantities using a database of cell survival experiments with ion beam irradiation *J. Radiat. Res.* **54** 494–514

Gonzalez-Lopez A, Vera-Sanchez J-A and Lago-Martin J-D 2015 Small fields measurements with radiochromic films *J. Med. Phys.* **40** 61–67

Grilj V and Brenner D J 2018 Let dependent response of gafchromic films investigated with mev ion beams *Phys. Med. Biol.* **63** 245021

Henthorn N T *et al* 2020 Mapping the future of particle radiobiology in europe: The inspire project *Front. Phys.* **8** 565055

Horst F *et al* 2025 The research beamlines at the dresden proton therapy facility: available infrastructure and experimental capabilities *Front. Oncol.* **15** 1594973

Howard M E, Herman M G and Grams M P 2020 Methodology for radiochromic film analysis using FilmQA Pro and imagej *PLoS One* **15** e0233562

Jones B, McMahon S and Prise K 2018 The radiobiology of proton therapy: challenges and opportunities around relative biological effectiveness *Clin. Oncol.* **30** 285–92

Karsch L, Beyreuther E, Burris-Mog T, Kraft S, Richter C, Zeil K and Pawelke J 2012 Dose rate dependence for different dosimeters and detectors: TLD, OSL, EBT films and diamond detectors *Med. Phys.* **39** 2447–55

Kato T 2019 Current status of dosimetry tools for clinical proton beams *Radiat. Environ. Med.* **8** 59–69
Kirby D, Green S, Fiorini F, Parker D, Romagnanin L, Doria D, Kar S, Lewis C, Borghesi M and Palmans H 2011 Radiochromic film spectroscopy of laser-accelerated proton beams using the FLUKA code and dosimetry traceable to primary standards *Laser Part. Beams* **29** 231–9
Lewis D, Micke A, Yu X and Chan M F 2012 An efficient protocol for radiochromic film dosimetry combining calibration and measurement in a single scan *Med. Phys.* **39** 6339–50
McNamara A L, Schuemann J and Paganetti H 2015 A phenomenological relative biological effectiveness (RBE) model for proton therapy based on all published in vitro cell survival data *Phys. Med. Biol.* **60** 8399–416
Méndez I, Rovira-Escutia J J and Casar B 2021 A protocol for accurate radiochromic film dosimetry using Radiochromic.com *Radiol. Oncol.* **55** 369–78
Metzkes-Ng J *et al* 2023 The dresden platform is a reserach hub for ultra-high dose rate radiobiology *Sci. Rep.* **13** 20611
Mijnheer B 2017 *Clinical 3D Dosimetry in Modern Radiation Therapy* (CRC Press)
Munshi A, Hobbs M and Meyn R E 2005 Clonogenic cell survival assay *Chemosensitivity: Volume 1 In Vitro Assays* pp 21–28
Niroomand-Rad A *et al* 2020 Report of AAPM task group 235 radiochromic film dosimetry: an update to TG-55 *Med. Phys.* **47** 5986–6025
Redondo-Cubero A, Borge M J G, Gordillo N, Gutiérrez P C, Olivares J, Pérez Casero R and Ynsa M D 2021 Current status and future developments of the ion beam facility at the centre of micro-analysis of materials in madrid *Eur. Phys. J. Plus* **136** 175
Resch A F, Heyes P D, Fuchs H, Bassler N, Georg D and Palmans H 2020 Dose- rather than fluence-averaged let should be used as a single-parameter descriptor of proton beam quality for radiochromic film dosimetry *Med. Phys.* **47** 2289–99
Romano F *et al* 2016 The ELIMED transport and dosimetry beamline for laser-driven ion beams *Nucl. Instrum. Methods Phys. Res. A* **829** 153–8
Rovituso M *et al* 2025 Characterisation of the hollandPTC R&D proton beamline for physics and radiobiology studies *Phys. Med.* **130** 104883
Sanchez-Parcerisa D *et al* 2021 Radiochromic film dosimetry for protons up to 10 MeV with EBT2, EBT3 and unlaminated EBT3 films *Phys. Med. Biol.* **66** 115006
Santos T, Ventura T and do Carmo Lopes M 2021 A review on radiochromic film dosimetry for dose verification in high energy photon beams *Radiat. Phys. Chem.* **179** 109217
Saur S and Frengen J 2008 GafChromic EBT film dosimetry with flatbed CCD scanner: a novel background correction method and full dose uncertainty analysis *Med. Phys.* **35** 3094–101
Suckert T, Nexhipi S, Dietrich A, Koch R, Kunz-Schughart L A, Bahn E and Beyreuther E 2021 Models for translational proton radiobiology—from bench to bedside and back *Cancers* **13** 4216
Unkelbach J, Botas P, Giantsoudi D, Gorissen B and Paganetti H 2017 Reoptimization of intensity-modulated proton therapy plans based on linear energy transfer *Int. J. Radiat. Oncol. Biol. Phys.* **96** 1097–106
Vadrucci M *et al* 2015 Calibration of Gafchromic EBT3 for absorbed dose measurements in 5 MeV proton beam and $^{(}60)$Co γ-rays *Med. Phys.* **42** 4678–84
Vallières S, Bienvenue C, Puyuelo-Valdes P, Salvadori M, d'Humières E, Schiettekatte F and Antici P 2019 Low-energy proton calibration and energy-dependence linearization of EBT-XD radiochromic films *Rev. Sci. Instrum.* **90** 083301
Xiao A Y *et al* 2019 Sodium sulfide selectively induces oxidative stress, dna damage and mitochondrial dysfunction and radiosensitizes glioblastoma (GBM) cells *Redox Biol.* **26** 101220